Bending energy of a vesicle to which a small spherical particle adhere: An analytical study*

Cao Si-Qin(曹思勤)[a], Wei Guang-Hong(韦广红)[a)†], and Jeff Z. Y. Chen[b)‡]

[a)] *State Key Laboratory of Surface Physics, Key Laboratory for Computational Physical Sciences (Ministry of Education), Department of Physics, Fudan University, Shanghai* 200433, *China*

[b)] *Department of Physics and Astronomy, University of Waterloo, Ontario N2L3G1, Canada*

(Received 22 January 2015; revised manuscript received 23 March 2015; published online 3 August 2015)

On the basis of Helfrich's bending energy model, we show that the adsorption process of a small spherical particle to a closed vesicle can be analytically studied by retaining the leading terms in an expansion of the shape equation. Our general derivation predicts the optimal binding sites on a vesicle, where the local membrane shape of the binding site could be non-axisymmetric before the continuous adhesion transition takes place. Our derivation avoids directly solving the shape equation and depends on an integration of the contact-line condition. The results are verified by several examples of independent numerical solutions.

Keywords: membrane conformation, Helfrich model, nano-particle adsorption, phase transition

PACS: 87.16.dt, 46.70.Hg, 68.03.Cd, 87.17.Aa **DOI:** 10.1088/1674-1056/24/9/098702

1. Introduction

The theoretical treatment of a membrane, either in an open conformation or in a closed vesicle conformation, is largely based on the bending-energy model that was originally proposed by Helfrich.[1] Insightful structures can be theoretically determined from this model, which are then used to describe experimental observations in membrane systems.[2,3] For example, free-vesicle shapes can be predicted from the model. In particular, those having an axisymmetry have been classified as a function of the vesicle's reduced volume

$$v = 6\sqrt{\pi}V/A^{3/2}, \tag{1}$$

where V is the internal volume and A is the surface area of a vesicle.[2,4,5] Three representative conformations (i.e., stomatocyte, oblate, and prolate) are illustrated in Fig. 1.

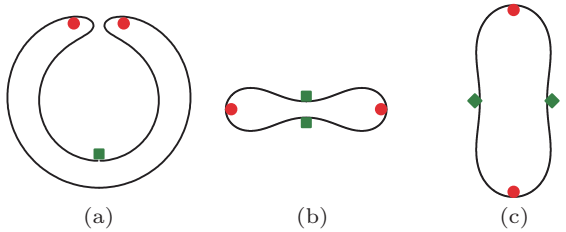


Fig. 1. (color online) Three representative conformations of a vesicle: a $v = 0.4$ stomatocyte (a), a $v = 0.6$ oblate (b), and a $v = 0.8$ prolate (c). According to the current work, the internal and the external adhesion sites are indicated by (red) circles and (green) squares, respectively, for a small spherical particle adhering to a stomatocyte (a), an oblate (b), and a prolate (c). The filled diamonds specify the equatorial line on a prolate that is further discussed in Section 3.5.

As an approximation, synthetic nano-particles and viruses that interact with a membrane surface are commonly modeled by a hard spherical particle.[6–8] In this paper, we examine the structure of a particle–membrane complex caused by particle–membrane adhesion. This adhesion is usually characterized by an attraction energy per unit area, w, acting between the particle and membrane surface on contact.[9] One important theoretical identity is the contact-line condition that connects the local membrane and substrate curvatures at the contact line to the adhesion strength w,[10] in a general form regardless of the original membrane shape and adhering particle geometry. This identity will be employed in Section 3.2 of the current work. The model system of a spherical particle adsorbing to a flat, deformable, and infinitely large membrane sheet was previously considered in order to illustrate many interesting concepts, such as the continuous adhesion transition and engulfing of the sphere by the membrane as w raises.[11–14]

The physical properties of the adhesion of a spherical particle to a vesicle has been explored by using computer simulations of a coarse-grained model,[15] and variational and numerical calculations of the bending energy model.[16–20] As it turns out, for an oblate vesicle, as w and the size of the adhering sphere change, an exact numerical solution to the bending energy model yields a rather rich phase diagram where multiple phases exist.[17] Adhesion of a small sphere to the internal surface would result in budding as w increases [Fig. 2(a)], or adhesion to the external surface would result in engulfing as w increases [Fig. 2(b)]. Within the length scale of an adhering

*Project supported by the National Natural Science Foundation of China (Grant Nos. 11074047 and 11274075), the Research Fund for the Doctoral Program of Higher Education of China (Grant No. RFDP-20100071110006), and the Natural Science and Science Engineering Council of Canada.

†Corresponding author. E-mail: ghwei@fudan.edu.cn

‡Corresponding author. E-mail: jeffchen@uwaterloo.ca

© 2015 Chinese Physical Society and IOP Publishing Ltd

sphere, the membrane appears large, thus locally these processes do not differ much from the simple picture of a sphere adhering to a flat membrane,[11–14] where the transition properties are controlled by a surface tension σ. Here, we focus on a system where the vesicle has a size which is much greater than the adhering sphere's radius. The adhesion site depends on the curvature of the vesicle where the small sphere approaches, which in turn influences the onset of the adhesion transition. As will be shown below, for such a problem, σ is no longer important.

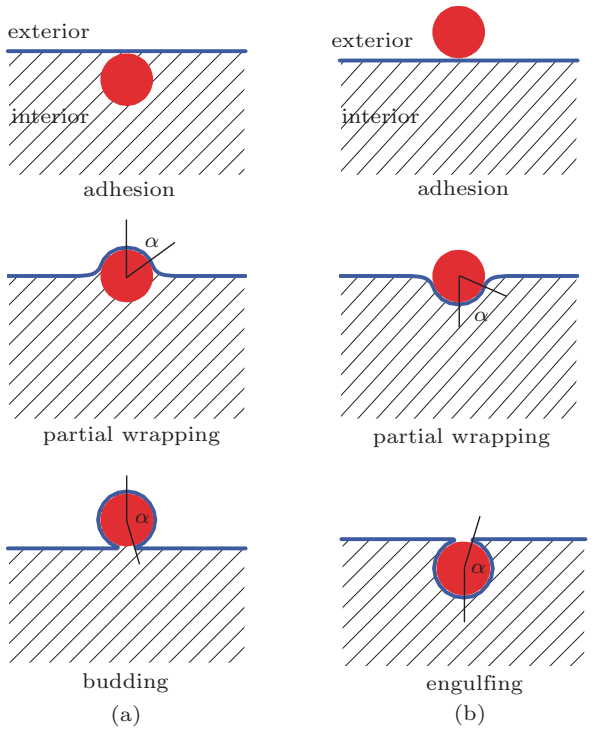


Fig. 2. (color online) (a) Conformations in a budding transition: adhesion of a sphere to the membrane from the interior of a vesicle, sphere partially wrapped by the membrane, and a budding state where the sphere is entirely wrapped by the membrane; (b) conformations in an engulfing transition: adhesion of a sphere to the membrane from the exterior of a vesicle, sphere partially wrapped by the membrane, and engulfing of the sphere by the membrane.

This paper is organized as follows. In Section 2, we adopt a general form of the bending energy model and will briefly review the resulting shape equation that governs curvature properties of the membrane.[23–26] In Section 3.1, with the consideration of a small adhering sphere, we argue that near the contact line the membrane displays a catenoid shape; regardless of the global, possibly non-axisymmetric vesicle shape, locally a symmetry axis can be chosen for the wrapping membrane on the small sphere. Some detailed mathematical derivations that back up the argument can be found in Appendices. In Appendix A, we set up a general coordinate system for the problem. In Appendix B, we expand the shape equation in terms of a small parameter, which does not depend on an axisymmetry coordinate setup that was used previously.[11–14,16,17,27,28] The result is an analytic expression for the membrane curvature at the contact line, which is presented in Section 3.1. In Appendix C, we show that the contact line on a small sphere is a circle. In Section 3.3, using the general contact-line condition, we analytically determine the bending energy of the non-adhering vesicle portion of a partially wrapped sphere-vesicle complex, the energy depends on the curvature of the initial adhesion site. According to these results, in Sections 3.4 and 3.5, we locate the adsorption sites for the adhesion–budding transition and adhesion–engulfing transition on a vesicle; some examples are specified in Fig. 1 by circles and squares. The numerical solution to the original free vesicle problem is then used to determine the adhesion phase transition and deep wrapping (budding and engulfing) boundaries in two examples. Our general analytic results, which are based on the approximation of a small particle radius, are validated in Sections 3.3 and 3.6 by comparing them with independent numerical solutions to the same problem without taking the approximation.[17]

2. Model

The total energy of the particle–membrane complex is composed of the membrane's bending energy, E_b, surface tension, and work of the osmotic pressure, E_s, as well as the particle–membrane interaction energy, E_a. The bending energy of the membrane is generally described by the curvature model[1–3]

$$E_\mathrm{b} = \int \frac{\kappa_\mathrm{b}}{2}(K - C_0)^2 \mathrm{d}A + \kappa_G \int G \mathrm{d}A, \tag{2}$$

where $K/2 = (C_1 + C_2)/2$ is the mean curvature, $G = C_1 C_2$ is the Gaussian curvature, and C_1 and C_2 are the two principle curvatures of the membrane surface element $\mathrm{d}A$. We consider the general case of a nonvanishing spontaneous curvature, C_0; for a symmetric bilayer lipid composition we set $C_0 = 0$ later.[29] The two bending moduli, κ_b and κ_G, together with C_0, are system dependent.

We consider the particle–vesicle adhesion interaction that does not yield any vesicle topological change. According to the Gauss–Bonnet theorem the last term in Eq. (2) is a constant. Instead of dropping that term, we explicitly keep it for consistency in the derivation given below. Normally, one assumes that the total surface area and the internal volume of the vesicle are fixed for a particular system. A mathematically equivalent treatment is given by the introduction of two Lagrangian multipliers, σ and p, to deal with the constraints. This amounts to an additional energy

$$E_\mathrm{s} = \sigma \int \mathrm{d}A + p \int \mathrm{d}V, \tag{3}$$

which has the physical meaning of surface-stretching energy and osmotic-pressure based work.

The adhesion energy is assumed to be proportional to the contact area A_C (i.e., the area of the spherical particle that is covered by the adhering membrane)

$$E_a = -wA_C, \tag{4}$$

where w is the attraction energy gain per unit area between the membrane and the particle's surface. A similar expression has been used in recent studies of related systems.[5,10,16,17,21,22,30–36] This energy becomes effective when the surfaces of the particle and membrane are in contact. Alternatively, one could use a potential-well based attraction scheme, such as those normally used in computer simulations,[21,22,37,38] where the attraction energy is a function of the distance between the surfaces. In the current approach, we use the more convenient contact attraction in Eq. (4) with the understanding that the two approaches are physically the same for a short-ranged potential well.

One can then take the sum of the above three energies and treat the problem by a variation method to minimize the total energy in order to determine the optimal vesicle shape. The shape of the free portion of the membrane is then described by the differential equation[23–26]

$$\nabla^2 K + \frac{1}{2}(K - C_0)(K^2 - 4G - C_0 K) = \sigma K + p, \tag{5}$$

where ∇^2 is the Laplacian operator.

3. Results and discussion

3.1. Membrane's curvature at the contact line of a small adsorbing sphere

In this subsection, we consider the contact line shape for adhesion to a small spherical particle having a radius R_p. When we say a "small" particle, we refer to the condition

$$KR_p \ll 1, \tag{6}$$

where $K/2$ is the mean curvature on any point of the nonadhered portion of the vesicle.

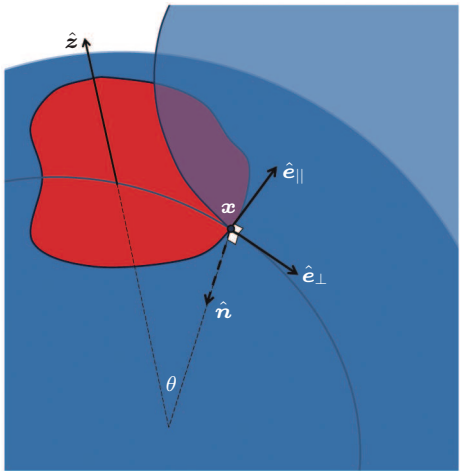


Fig. 3. (color online) An arbitrary contact line on the surface of a sphere where part of the sphere is partially wrapped by the (blue) membrane.

The contact line forms a loop (of an arbitrary shape for now) on the surface of the (red) sphere, as shown in Fig. 3. At any point $\boldsymbol{X}$ on the contact line: a unit vector tangent to the contact line specifies the parallel ($\parallel$) direction, $\hat{\boldsymbol{e}}_{\parallel}$; a unit vector normal to the plane locally tangent to both membrane and adsorbing hard surfaces at $\boldsymbol{X}$ specifies the surface normal, $\hat{\boldsymbol{n}}$; and finally, a unit vector normal to both $\hat{\boldsymbol{e}}_{\parallel}$ and $\hat{\boldsymbol{n}}$ specifies $\hat{\boldsymbol{e}}_{\perp}$.

According to differential geometry two curvatures, $K_{\perp}$ and $K_{\parallel}$, can be defined along $\hat{\boldsymbol{e}}_{\perp}$ and $\hat{\boldsymbol{e}}_{\parallel}$. The mean curvature $K/2$ can then be expressed through

$$K = K_{\perp} + K_{\parallel}. \tag{7}$$

As already discussed in Refs. [10] and [39], crossing the contact line by following the $\hat{\boldsymbol{e}}_{\perp}$ direction, $K_{\perp}$ is discontinuous from the unadsorbed membrane portion to the adsorbed portion. On the other hand, crossing $\boldsymbol{X}$ following the contact curve, $K_{\parallel}$, is continuous.

The surface normal of the adsorbing sphere at $\boldsymbol{X}$ is the same as the radial direction $\hat{\boldsymbol{r}}$, directing from the center of the sphere to $\boldsymbol{X}$. Because $\hat{\boldsymbol{n}}$ at $\boldsymbol{X}$ is a joint surface normal for both the membrane and substrate surfaces

$$\hat{\boldsymbol{n}} = -\hat{\boldsymbol{r}}. \tag{8}$$

Therefore, $\hat{\boldsymbol{n}}$ and $\hat{\boldsymbol{e}}_{\parallel}$ defines a great circle on the spherical surface, from which we have

$$K_{\parallel} = 1/R_p. \tag{9}$$

This is actually true for any R_p size.

Now consider the unadsorbed side of the membrane emerging from $\boldsymbol{X}$. Taking Eqs. (7) and (9), we have

$$R_p K_{\perp} = -R_p K_{\parallel} + R_p K = -1 + R_p K. \tag{10}$$

In the current small sphere system, from Eq. (6), we can drop the $R_p K$ term, hence $K_{\perp} \simeq -K_{\parallel} = -1/R_p$. This implies that the membrane shape at the contact line is a catenoid surface. A few interesting features immediately emerge.

First, $K_{\parallel} = 1/R_p$ is a constant along the entire contact line. This property, together with an asymptotic solution of Eq. (5) in the small-R_p limit, guarantees that the contact line is a circle on the particle's surface [see Appendices A, B, and C]. Although the parametrization so far is for a general, non-axisymmetric case, this means that a new, local z axis can be established, about which the membrane near the contact line is axisymmetric. At a larger scale, the entire vesicle shape need not be axisymmetric.

Next, following such a local axisymmetric setup, the location of the contact circle on the sphere is uniquely defined by the parameter θ, from which $\alpha = \pi - \theta$ can now be interpreted as the wrapping angle on a spherical adsorbing substrate. In

Appendix B, solving Eq. (5) we show that the membrane curvature K at the contact line follows:

$$K - C_0 = A\cos\alpha + \mathcal{O}(R_p K^2), \tag{11}$$

where A is a constant that does not depend on the wrapping angle. The terms that were neglected have the order of magnitude $\mathcal{O}(R_p K^2)$. The constant A can be determined by considering the special case, $\alpha = 0$, which gives $A = K_0 - C_0$, where K_0 is the curvature when the membrane just touches the adsorbing sphere at a vanishing wrapping angle. In this work, we focus on the case that the adhesion transition is continuous, which implies that K changes continuously before and after the adhesion transition taking place at $\alpha = 0$. Hence, we can write

$$K - C_0 = (K_0 - C_0)\cos\alpha, \tag{12}$$

where K_0 can be understood as the curvature of the membrane before the particle is adhered. This curvature, of course, depends on the location on the vesicle that the particle adheres to.

3.2. Contact-line condition

The contact-line condition

$$w = \frac{\kappa_b}{2}(K_\perp - \underline{K}_\perp)^2 \tag{13}$$

relates the adsorption energy w to $K_\perp$ of the membrane on the two sides of the contact line, $K_\perp$ on the unadsorbed side and $\underline{K}_\perp$ on the adsorbed side. The relationship was derived by Seifert and Lipowsky[10] as well as Deserno.[39] For an adsorbing sphere, $\underline{K}_\perp = 1/R_p$. Using $K_\perp \equiv K - K_\parallel = K - 1/R_p$ we have

$$w = \frac{\kappa_b}{2}\left(K - \frac{2}{R_p}\right)^2. \tag{14}$$

So far, this condition is for any size of adsorbing sphere. Taking the small sphere result, equation (12), we then have

$$\frac{wR_p^2}{4\kappa_b} = \frac{1}{2}\left[1 - b_0 - (a_0 - b_0)\cos\alpha\right]^2, \tag{15}$$

where $a_0 = K_0 R_p/2$ and $b_0 = C_0 R_p/2$.

3.3. Bending energy of the vesicle–particle complex

Now, we consider a variation process where the contact area A_C between the membrane and particle varies, and the bending energy δE_b changes due to the vesicle distortion caused by adhesion. The total energy must remain minimum

$$\delta E = \delta E_b - w\delta A_C = 0, \tag{16}$$

which is an condition that was considered previously.[10,39] This expression can be used as the basis for arriving at a general procedure of calculating the bending energy $E_b(A_C)$. By integrating this expression, we have

$$E_b(A_C) - E_b(0) = \int_0^{A_C} w\,\mathrm{d}A, \tag{17}$$

where $E_b(0)$ is the original vesicle energy before the adsorption takes place.

The integrand in the above, w, is already given in Eq. (15) as a function of α. Considering the relationship between A and α

$$A(\alpha) = 2\pi R_p^2(1 - \cos\alpha), \tag{18}$$

we can carry out the integral and obtain

$$\frac{\Delta E_b}{8\pi\kappa_b} = (1 - b_0)^2\frac{A_C}{4\pi R_p^2} + \frac{\Delta E_b^f}{8\pi\kappa_b} + \mathcal{O}[a_0^2, b_0^2], \tag{19}$$

where $\Delta E_b = E_b(A_C) - E_b(0)$ is the difference between the bending energy of the particle–membrane complex and the vesicle energy before the adsorption. The first term on the right-hand side of Eq. (19) is the membrane's bending energy associated with the contact area A_C and the second term is the energy of the unattached potion of the vesicle, ΔE_b^f, where

$$\frac{\Delta E_b^f}{8\pi\kappa_b} = -\frac{R_P(K_0 - C_0)}{4}\frac{A_C}{2\pi R_p^2}\left(2 - \frac{A_C}{2\pi R_p^2}\right). \tag{20}$$

Valid for small-particle adsorption, the bending energy difference, equation (19), was obtained without the explicit consideration of calculating the membrane shape curve, which has been done previously.[5,10,16,17,30–36] Note that a_0, through K_0, is adhesion-site specific. This general expression is suitable for any adhesion site on the vesicle, where the site could be a locally non-axisymmetric point. Another interesting point is that the Lagrangian multipliers σ and p that were introduced in the earlier stage of the theory have now disappeared in the final result. This surprising conclusion can be traced back to solving Eq. (5): by taking a small R_p limit, the terms associated with σ and p disappear in an order-of-magnitude estimation, as presented in Appendix B. The net effects of σ and p on the original problem of the considered vesicle (before particle adhesion) still remain and they determine the stable free vesicle shape.[2,5]

Equation (20) is a remarkable analytic result, which states that the bending energy of the unattached portion is a quadratic function of the reduced contact area $A_C/2\pi R_p^2$, having a maximum magnitude

$$\frac{\Delta E_b^f}{8\pi\kappa_b} = -\frac{R_p(K_0 - C_0)}{4} \tag{21}$$

at half wrapping when $A_C^{\max} = 2\pi R_p^2$ (or $\alpha^{\max} = \pi/2$). The sign of this energy is completely determined by the sign of $K_0 - C_0$.

To validate this result, we consider two examples, both having $C_0 = 0$. As previously known, the free vesicle shape

is completely controlled by a dimensional characteristic number of the vesicle, the reduced volume in Eq. (1). We considered two special cases, $v = 0.6$ and $v = 0.95$, corresponding to an oblate vesicle and a prolate vesicle, respectively. We have solved the adsorption problem following the numerical procedure described in our previous paper,[17] without any of the analytic consideration explained above. The adsorption sites for both cases were selected at the axisymmetric axis of the vesicle (the "north pole"), where $K_0\sqrt[3]{3V/4\pi}/2 = 0.947$ and $K_0\sqrt[3]{3V/4\pi}/2 = -1.461$, respectively, for the two cases, $v = 0.6$ and $v = 0.95$. For each case, three values of the dimension ratio

$$y \equiv (3V/4\pi)^{1/3}/R_{\rm p} \tag{22}$$

are considered in the numerical solution.

The parameter y measures the relative size of the vesicle in comparison with the radius of the adsorbing spheres. We expect that asymptotically large y data converge to our theoretical prediction. In Fig. 4, we plot the numerical data by triangles ($y = 21.5$), squares ($y = 36.8$), and circles ($y = 46.4$). The two examples, $v = 0.6$ and $v = 0.95$, are shown by filled and open symbols in the figure. As the particle's radius is reduced (or y increases), we can see that the numerical results converge to the theoretical curves for small $R_{\rm p}$, equation (20), plotted as the solid curve for $v = 0.95$ and dashed curve for $v = 0.6$.

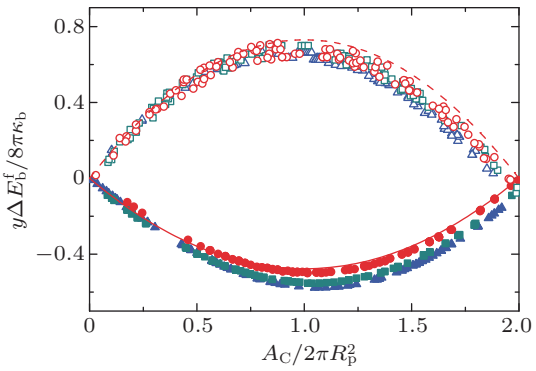


Fig. 4. (color online) Comparison between the numerical results (symbols) and the theoretical prediction (lines) of the bending energy change for the unattached membrane portion, $\Delta E_{\rm b}^{\rm f}/8\pi\kappa_{\rm b}$, as a function of the reduced wrapping area, $A_{\rm C}/2\pi R_{\rm p}^2$. Two example vesicles are considered: $v = 0.6$ (filled symbols) and $v = 0.95$ (open symbols). The numerical results were obtained by solving the shape equation exactly;[17] the theoretical prediction, equation (19), is made by an expansion on the small particle radius. Triangles, squares, and circles correspond to vesicle to particle dimension ratio, $y = 21.5, 36.8$, and 46.4, respectively. The dotted horizontal lines represent a typical thermal energy of order $k_{\rm B}T$, whereas the bending modulus $\kappa_{\rm b}$ is taken here to be $\approx 10k_{\rm B}T$ (the value of POPC reported in Ref. [40]); for different y the same color is used here.

We have demonstrated here that our exact solution can be validated by the numerical solution, which are both obtained on the assumption that the thermal fluctuations can be ignored. An interesting question is: how useful is the plot in this figure in comparison with a real system where the thermal fluctuations exist? A typical thermal energy $k_{\rm B}T$ can be compared with $\kappa_{\rm b}$ by $\kappa_{\rm b} \sim 10k_{\rm B}T$. In Fig. 4, we illustrate the typical thermal energy by dotted lines. In most of the parameter region, our theoretical expression should be unaffected by thermal fluctuations.

3.4. Internal adhesion and budding transition

We first discuss the predicted physics of internal adhesion, which eventually results in the budding of a small particle to the interior wall of a vesicle, using the derivation in the above sections. For simplicity, we only consider membranes without spontaneous curvature, $C_0 = 0$. Before adhesion, the vesicle is in a free vesicle state, which is a problem that was previously studied by Seifert *et al.*[15] according to the bending energy model, Eq. (2). The stable structure depends on a single geometric parameter. In the reduced volume v in Eq. (1), the stomatocyte is stable within the range $v = (0, 0.5915]$, oblate $v = [0.5915, 0.6516]$, and prolate $v = [0.6516, 1]$. Figure 1, without the additional marked symbols, illustrates the shape of these structures at $v = 0.4, 0.6$, and 0.8.

Note that K_0 is defined from the adhering particle side. For the current case, it differs by a sign from the case where the particle adheres from the exterior of the vesicle. At the beginning of the adhesion transition, the contact area $A_{\rm C}$ is asymptotically small. To minimize the energy in Eq. (20), the particle seeks an interior site where K_0 is concave and has the maximal curvature K_0^*. A few examples of the curvature of the unperturbed vesicle, K_0, are illustrated in Appendix D, where K_0^* is indicated by a red dot. This identifies the preferred internal adhesion sites, labeled by (red) circles in Fig. 1. In both stomatocyte ($v = 0.4$) and oblate ($v = 0.6$), the adhesion sites form a circle about the overall-shape symmetric axis. The local sites are not axisymmetric before adhesion takes place. In a cross section view of a stomatocyte, the most concave points appear at a place with C_1 is maximum, which is different from the actual place where $K_0 = C_1 + C_2$ is the maximum.

The continuous internal adhesion transition can then be determined by letting the wrapping angle $\alpha \to 0$ in Eq. (2). By re-arranging the quantities, we obtain the transition adhesion energy, $w_{\rm ad}$, in

$$[(w_{\rm ad}R_{\rm p}^2/2\kappa_{\rm b})^{1/2} - 1]y = K_0(3V/4\pi)^{1/3}/2. \tag{23}$$

The quantities in this expression have been arranged so that the right hand side does not contain the particle size $R_{\rm p}$. The dimensionless $K_0V^{1/3}$ can be calculated from a numerical solution to the free vesicle problem[5,17] and is plotted in Fig. 5 by the dotted curve. Below $w_{\rm ad}$ the system is in a desorbed state, while above $w_{\rm ad}$ the system is in a partially wrapped state. At the onset of the transition when $w = w_{\rm ad}$, the vesicle shape changes continuously from those plotted in the figure to enable a non-trivial wrapping angle.

As w increases beyond $w_{\rm ad}$, more of the area of the sphere is covered by the wrapping membrane, until the wrapping area reaches the full wrapping value, $A_{\rm C} = 4\pi R_{\rm p}^2$, at which $\alpha = \pi$. In this particular case, the small sphere is completely wrapped, forming a bud at the adhesion site. The same Eq. (15) can be used to determine the onset of the budding transition by setting $\alpha = \pi$

$$[(w_{\rm bud}R_{\rm p}^2/2\kappa_{\rm b})^{1/2} - 1]y = -K_0(3V/4\pi)^{1/3}/2. \qquad (24)$$

Note that the right hand side of this equation has a sign difference from Eq. (23). The conformation of a budding particle–membrane complex can be recovered from the analytic analysis. Because of the small volume $V_{\rm p}$, the nonadhered portion of the vesicle has a volume $V' = V - V_{\rm p} \simeq V$ and a surface area $A' = A - A_{\rm p} \simeq A$. Given the fact that the shape curve now closes with a wrapping angle $\alpha = \pi$, the nonadhered vesicle portion has an identical shape as the original, free vesicle. Some example configurations are illustrated in Fig. 5 near the budding boundary, $w_{\rm bud}$, which is represented by the dashed curve.

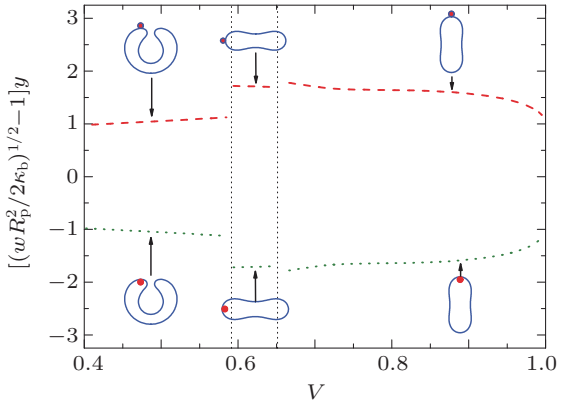


Fig. 5. (color online) The adhesion–budding phase boundaries analytically determined in the current work. The dotted line divides the desorbed state and adhesion state, according to Eq. (23). The dashed line divides the adhesion state and the budding state, according to Eq. (24).

3.5. External adhesion to vesicle and engulfing transition

In this section, we discuss the consequences of applying Eq. (19) to the case of external adhesion of a small adhering spherical particle to the outside layer of a vesicle. For simplicity, we again focus on the case of no spontaneous curvature, $C_0 = 0$ [or $b_0 = 0$ in Eq. (19)].

The optimal adhesion site on the vesicle can then be predicted based on Eq. (19) for both a stomatocyte or oblate. Because K_0, hence a_0 in Eq. (19) is site-dependent, and we can search for the most concave ($K_0 > 0$) site where K_0 is a maximum. The (green) squares in Fig. 1 specify these sites for these two typical cases.

Here, we assume that the adhesion transition is continuous such that at the transition α starts from 0. Using $\alpha = 0$ in Eq. (15) we can then predict that the adhesion transition takes place as w increases to $w_{\rm ad}$, where $w_{\rm ad}$ is given in Eq. (23). The dotted curve in Fig. 6 illustrates this phase boundary.

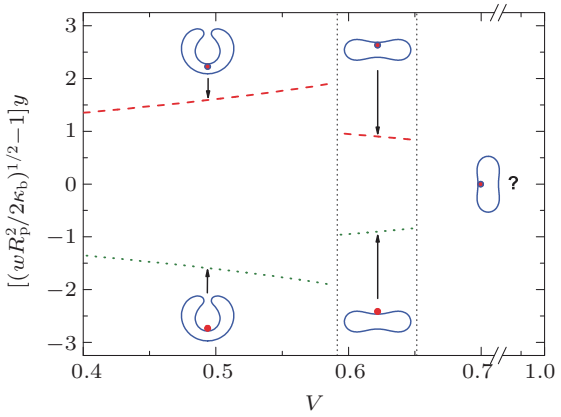


Fig. 6. (color online) The adhering–engulfing phase boundaries analytically determined in this work. The dotted line separates the desorbed and adhesion states, while the dashed line separates the adhesion and engulfing states. The phase behavior in the prolate region is unknown from the current work.

As w goes beyond $w_{\rm ad}$, the sphere starts to become partially wrapped by the membrane. The fully wrapped, i.e., engulfing state, is reached when $A_{\rm C}$ becomes $4\pi R_{\rm p}^2$, or $\alpha = \pi$ for a small spherical particle. The onset of engulfing, $w_{\rm eng}$, can be determined from the same equation as in Eq. (24)

$$[(w_{\rm eng}R_{\rm p}^2/2\kappa_{\rm b})^{1/2} - 1]y = -K_0(3V/4\pi)^{1/3}/2. \qquad (25)$$

The long-dashed curve in Fig. 6 indicates the engulfing boundary. For a small sphere, $V_{\rm p} \ll V$ and $A_{\rm p} \ll A$, the much larger portion of the newly closed vesicle forms a conformation that is identical to the original free vesicle shape, as illustrated by the conformation in the same figure near the engulfing boundary.

We assumed that the initial adhesion transition is continuous, which has been demonstrated in a number of related systems where the numerical and analytical solutions to the bending energy model were obtained.[10,16,17,30–36] In all of these cases, including those discussed in the last section and the two examples (stomatocyte and oblate) cited above, the adhesion sites on the original vesicle are either concave or flat, as approached from the adhesion side.

The analysis, however, becomes problematic when generalized to the case of small particle adhesion to a prolate (Fig. 1). Although some regions of the prolate shape curve look concave in the cross section view, figure 1, the entire three-dimensional vesicle shape is actually convex ($K_0 < 0$). According to Eq. (19), we would conclude that the adhesion transition takes place at a site where $-K_0$ is minimal, or $|K_0|$ is the smallest. The "equator" line on the prolate, as illustrated in Fig. 1 by two diamonds, is the location qualifying the requirement. Taking it further, we would also predict that engulfing takes places at a value specified by Eq. (25). Because $K_0 < 0$,

according to Eqs. (23) and (25), $w_{\rm eng} < w_{\rm ad}$, in a reversed order in comparison with the examples discussed above. Hence, as w increases, the system would first undergo a discontinuous engulfing transition and then the wrapping angle would decrease as w increases. This rather unphysical consequence is not self-consistent with the basic assumption used in our theoretical analysis, which states that a continuous adhesion transition is followed by engulfing at a larger w. Hence, we cannot directly use the current theory for the prolate desorption–adhesion–engulfing transitions.

3.6. Comparison with the numerical solution

The main theoretical results in this work, equations (15) and (19), were analytically derived based on: (i) a small-$R_{\rm p}$ expansion of the shape equation [Eq. (11)], (ii) the contact line condition [Eq. (13)], and (iii) the assumption that the adhesion transition is continuous. For the problem of particle adhesion to a vesicle with an axisymmetry, we can solve the original problem numerically without these assumptions, independent of any derivation in this paper, starting from the same bending energy model.[17] A comparison between the current analytical results and the independent numerical results would validate both approaches, particularly (i)–(iii) given above.

Using the computational method documented in our previous publication, we can draw the phase boundary completely on the basis of numerically comparing the magnitude of the calculated total energy of the system at different w for various $R_{\rm p}$. One example is for an oblate, $v = 0.6$, for which the continuous adhesion boundary and engulfing boundary were previously determined[17] and is redrawn in Fig. 7 by squares and circles, respectively. Also shown are the adhesion (dotted) and engulfing (dashed) lines determined from the current analytic approach. There is an excellent agreement between the results from the two, approaching the large $V/V_{\rm p}$ limit.

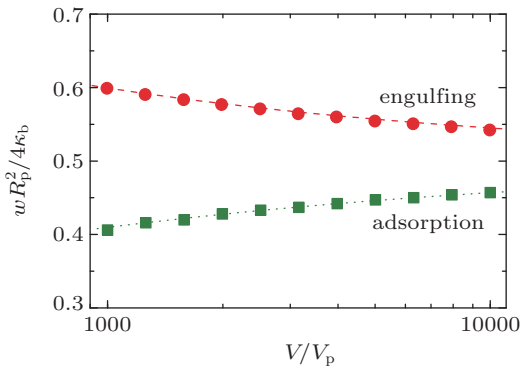


Fig. 7. (color online) Comparison between the theoretical adsorption and engulfing boundaries Eq. (15) ($b_0 = 0$, $\theta = 0$) and the numerical results for the adsorption of a particle and a $v = 0.6$ oblate vesicle. The numerical results, represented here by circles and squares, were obtained in the same way as in our previous paper.[17]

4. Summary

Starting from a general coordinate setup, we demonstrated that for an adhering small spherical particle the contact line that defines the wrapping edge of a membrane is a perfect circle on the sphere. This defines a local symmetric axis, although at a larger scale the vesicle could be in a non-axisymmetric shape. We showed how the total energy of the system consisting of a vesicle and an adhering small spherical particle can be obtained analytically from the properties of the mean curvature near the contact line. The result connects the energy with the originally unperturbed vesicle curvature, which can be calculated separately. For a vesicle made of lipid bilayer with no spontaneous curvature, we showed that the energetically preferred adhesion sites are those most concave positions on the original vesicle. We also generally determined the adhesion, engulfing, and budding boundaries for a vesicle, except for the adhesion-engulfing transition of a small particle to a prolate.

Our entire analysis was built on the basis of taking the leading order in the expansion of the shape equation on a small parameter $R_{\rm p}K_0$, where $R_{\rm p}$ is the radius of the spherical particle and K_0 is a typical membrane curvature. The analytic results were verified by a number of examples, where the numerical solution independent of the current approach is available.

The conformations of some states studied in this paper are similar to those found in biological processes, such as endocytosis and exicytosis. Given that biological systems are much more complicated, the successful application of the current work in these processes remains to be seen.

Appendix A: Coordinate system

To discuss a number of membrane properties in the following Appendices, we need to specify a general orthonormal coordinate system for describing the shape of the membrane. To start, we assume that a Cartesian coordinate system establishes the x and z axes in space.

We consider the plane that contains the z axis and a point on the membrane, $\boldsymbol{X}$. Such a plane makes an angle ϕ from the xz plane and contains an intersecting curve by cutting through the membrane surface [see Fig. A1]. Along the intersecting curve the point $\boldsymbol{X}$ is a contour distance u away from a previously defined origin. These two measures, u and ϕ completely determine the location of a point $\boldsymbol{X}$ on the membrane: $\boldsymbol{X} = \boldsymbol{X}(u, \phi)$. At $\boldsymbol{X}$, we can define a tangent plane of the membrane, which makes an angle θ from the plane normal to the z axis at point $\boldsymbol{X}$. A tangent vector $\hat{\boldsymbol{u}}$ can then also be defined as a function of u and θ. The direction of increasing ϕ is defined as $\hat{\boldsymbol{e}}_\phi$.

Two normal curvatures can be defined according to this setup. As the perpendicular and parallel components, $K_\perp$ can

be defined as the curvature along $\hat{\boldsymbol{u}}$, and $K_{\parallel}$ can be defined as the curvature along $\hat{\boldsymbol{e}}_{\phi}$. The mean curvature $K/2$ can be expressed through

$$K = K_{\perp} + K_{\parallel}. \tag{A1}$$

At this stage, the general coordinate setup does not depend on any possible underlying symmetry of the system.

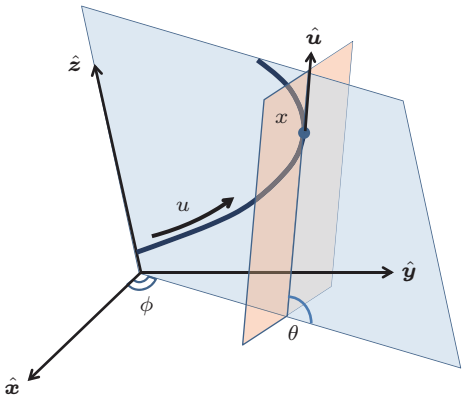


Fig. A1. (color online) The definition of the coordinate system that describes an arbitrary point $\boldsymbol{X} = \boldsymbol{X}(u,\phi)$ on the unbinded membrane surface. Two parameters, u and ϕ, are described in Appendix A. The general setup does not imply an axisymmetry about the z-axis.

Appendix B: Expansion of the shape equation

The general coordinate system, shown in Fig. A1, is established on the basis of orthonormal frame $\{\boldsymbol{e}_{\phi}, \boldsymbol{e}_u, \boldsymbol{n}\}$, where $\boldsymbol{n}$ is the normal vector of the membrane surface at $\boldsymbol{X}$. The Laplacian operator

$$\nabla^2 = \partial_u^2 + \frac{\cos\theta}{x}\partial_u + \frac{1}{x^2}\partial_{\phi}^2 \tag{B1}$$

can then be written. Instead of using u, it is convenient to directly use θ, so that $\partial_u = K_{\perp}\partial_{\theta}$ where $K_{\perp} = \boldsymbol{n}\cdot\partial_u\boldsymbol{e}_u$.[25,26]

In this appendix, we take an expansion of the shape equation in terms of a parameter so that the leading term can be analyzed asymptotically. Assuming that $K/K_{\perp}$ is a small parameter, we have

$$\begin{aligned} 0 = {} & \partial_{\theta}^2 K' + \frac{\cos\theta}{\sin\theta}\left(1 - \frac{K}{K_{\perp}}\right)^2 \partial_{\theta}K' + 2K' + \frac{1}{x^2K_{\perp}^2}\partial_{\phi}^2 K' \\ & + \frac{K}{K_{\perp}}\left\{\frac{(\partial_{\theta}K')^2}{K} - 2K'\right\} \\ & + \frac{K^2}{K_{\perp}^2}\left\{K' - \frac{C_0K'}{K} - \frac{\sigma K + p}{K^2}\right\}, \end{aligned} \tag{B2}$$

where $K' = K - C_0$. The justification of assuming a small $K/K_{\perp}$ will be discussed near the end of the next appendix.

According to the contact line condition in Eq. (14), for a given w, K is a constant along the contact line; hence, $\partial_{\phi}^2 K' = 0$. Now, we examine the portion of the free membrane that is asymptotically close to the contact line. Keeping the leading-order terms in Eq. (B2), we have

$$\partial_{\theta}^2 K' + \frac{\cos\theta}{\sin\theta}\partial_{\theta}K' + 2K' = 0. \tag{B3}$$

The general solution of this equation is

$$K'(\theta) = A\cos\theta + B\left\{\frac{\cos\theta}{2}\ln\frac{1+\cos\theta}{1-\cos\theta} - \frac{1}{2}\right\}, \tag{B4}$$

which contains two constants A and B, to be fixed by boundary conditions. At $\theta = 0$ or π, the expression inside the curry brackets diverges if $B \neq 0$. To ensure the finiteness of the curvature at any θ, we hence must have $B = 0$. The solution of this partial differential equation is then

$$K - C_0 = A\cos\theta, \tag{B5}$$

where A is an integration constant, which does not depend on the location of the contact point. Physically, going back to the discussion in the text, $\theta = 0$ and $\theta = \pi$ correspond to weak-wrapping and full wrapping of membrane on the spherical particle, respectively. The equation is valid for the asymptotic limit specified by Eq. (6) only. In practice, as shown by Fig. 4 and Fig. 7 against the numerical solution, the solution is already very accurate when $K_0R_{\rm p}$ is as small as 10^{-1}.

One interesting property is that both σ and p terms are associated with the second-order correction in the above expansion. The values of σ and p determine the original vesicle shape and can be treated as constant in the small $R_{\rm p}$ expansion. Dropping the second-order term completely erases the contribution from σ and p.

Appendix C: Shape of the contact line

The relationship between the membrane curvature K and the tangent plane angle θ given in Eq. (B5) is a general result for the free membrane portion at the contact line, without the assumption of the contact-line shape [see Fig. 3]. Because both K and C_0 are constant along the contact line, we can immediately draw the conclusion that the membrane angle θ is also a constant along the complete loop of the contact line.

The contact line is embedded on the membrane. Its line curvature $K_{\rm C}$ is related to the membrane curvature $K_{\parallel}$ by

$$K_C = K_{\parallel}/\sin\theta = 1/(R_{\rm p}\sin\theta). \tag{C1}$$

Following the discussion in the last paragraph, we know that the line curvature is a constant around the contact-line loop. Realizing that the contact line also belongs to the spherical surface, we can directly use the Frenet–Serret formulas, which state that a constant-curvature loop on a sphere is a circle.

Having established that the contact-line shape is a circle, we can define a local symmetry axis that goes through the sphere's center and is along the normal to the circular contact line. In the immediate local region, the membrane shape is asymptotically symmetric.

Examining the definition of θ in Fig. 3 and the wrapping angle in Fig. 2, we then arrive at Eq. (11) in Section 3.1. By taking the order-of-magnitude estimate in Eqs. (6) and (10), we see that $K/K_{\perp}$ is small so that the $K/K_{\perp}$ and $K^2/K_{\perp}^2$ terms are negligible in Eq. (B2).

Appendix D: Curvature of an unperturbed vesicle

The theory in this paper considers that the adsorption site on a vesicle, to which a small sphere adhere, is related to the curvature properties of an unperturbed vesicle K_0. In this section, we illustrate a few typical examples of K_0, on the basis of a numerical solution to the free vesicle problem.[5]

The original free vesicle problem contains an axisymmetry which allows for a cross section plot of the shape curve, as shown in Fig. D1. An arc variable s can be defined, ranging from $s = 0$ to $s = 1$, which identifies the two intersection points of the shape curve with the vertical axis. The curvature K_0, in reduced units, are plotted by the solid curves in the figure for a number of examples. Viewing from outside the vesicle, the most convex sites, where a negative K_0 reaches minima, are indicated in Figs. D1(a)–D1(c) by (red) circles. The most concave sites, where a positive K_0 reaches a maxima, are indicated in Figs. D1(d) and D1(e) by (green) squares. The least convex sites, where a negative K_0 reaches maxima are indicated in Figs. D1(d) and D1(e) by (green) diamonds.

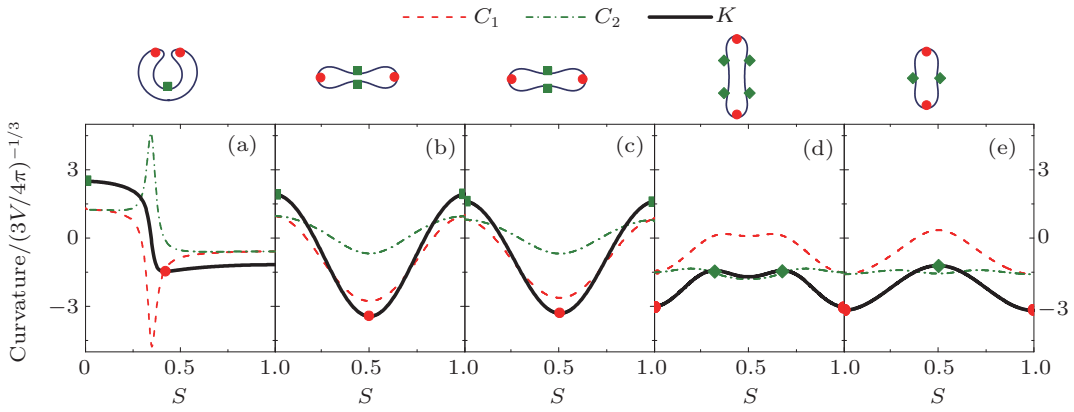


Fig. D1. (color online) Reduced curvature of a unperturbed vesicle as a function of the arc variable s for five typical examples: (a) $v = 0.591$ (stomatocyte), (b) $v = 0.591$ (oblate), (c) $v = 0.651$ (oblate), (d) $v = 0.651$ (prolate), and (e) $v = 0.8$ (prolate). The solid curves represent $K_0 = C_1 + C_2$, where C_1 and C_2 are the two principle curvatures plotted by the dashed and dot-dashed curves, respectively.

The same symbols are used to specify the locations on the shape curves above the plotted figures. The shape curve is shown in a cross section plot; however, this is sometimes deceiving because its shape only corresponds to C_1, one of the two principle curvatures. The minimum of the dashed curve in Fig. D1(a), which we would visually identify as the most concave point, is different from the actual minimum on the solid curve. The maxima of the dashed curves in Figs. D1(d) and D1(e) represent convex curvatures in a cross section view; however, at these locations the curvature is actually convex (negative).

References

[1] Hefrich W 1973 *Z. Naturforsch. C* **28** 693
[2] Seifert U 1997 *Adv. Phys.* **46** 13
[3] Muller M, Katsov K and Schick M 2006 *Phys. Rep.* **434** 113
[4] Deuling H J and Helfrich W 1976 *J. Phys.* **37** 1335
[5] Seifert U, Berndl K and Lipowsky R 1991 *Phys. Rev. A* **44** 1182
[6] Pelkmans L, Kartenbeck J and Helenius A 2001 *Nature Cell Biol.* **3** 473
[7] Sieczkarski S B and Whittaker G R 2002 *J. Gen. Viro.* **83** 1535
[8] Pietiainen V, Marjomaki V, Upla P, Pelkmans L, Helenius A and Hyypia T 2004 *Mol. Biol. Cell* **15** 4911
[9] Seifert U 1991 *Phys. Rev. A* **43** 6803
[10] Seifert U and Lipowsky R 1990 *Phys. Rev. A* **42** 4768
[11] Deserno M 2004 *Phys. Rev. E* **69** 31903
[12] Nowek S A and Chou T 2008 *Phys. Rev. E* **78** 021908
[13] Deserno M and Bickel T 2003 *Europhys. Lett.* **62** 767
[14] Deserno M 2004 *J. Phys.: Condens. Matter* **16** S2061
[15] Noguchi H and Takasu M 2002 *Biophys. J.* **83** 299
[16] Deserno M and Gelbart W M 2002 *J. Phys. Chem. B* **106** 5543
[17] Cao S, Wei G H and Chen J Z Y 2011 *Phys. Rev. E* **84** 050901
[18] Niu Y Q, Wei W, Zheng B, Zhang C X and Meng Q T 2014 *Acta Phys. Sin.* **63** 038701 (in Chinese)
[19] Zheng B and Meng Q T 2014 *Chin. Phys. B* **23** 038701
[20] Niu Y Q, Wei W, Zheng B, Zhang C X and Meng Q T 2013 *Chin. Phys. B* **22** 128701
[21] Zhang J, Das S and Du Q 2009 *J. Comp. Phys.* **228** 7837
[22] Zhao Y, Das S and Du Q 2010 *Phys. Rev. E* **81** 041919
[23] Ou-Yang Z C and Helfrich W 1987 *Phys. Rev. Lett.* **59** 2486
[24] Ou-Yang Z C and Helfrich W 1989 *Phys. Rev. A* **39** 5280
[25] Capovilla R and Guven J 2002 *J. Phys. A* **35** 6233
[26] Guven J 2004 *J. Phys. A* **37** L313
[27] Benoit J and Saxena A 2007 *Phys. Rev. E* **76** 041912
[28] Góźdź W T 2007 *Langmuir* **23** 5665
[29] Zimmerberg J and Kozlov M M 2006 *Nature Rev. Mol.* **7** 9
[30] Weikl T R 2003 *Eur. Phys. J. E* **12** 265
[31] Muller M M, Deserno M and Guven J 2005 *Euro. Phys. J.* **69** 482
[32] Muller M M, Deserno M and Guven J 2007 *Phys. Rev. E* **76** 011921
[33] Das S and Du Q 2008 *Phys. Rev. E* **77** 011907
[34] Chen J Z Y, Liu Y and Liang H J 2009 *Phys. Rev. Lett.* **102** 168103
[35] Mkrtchyan S, Ing C and Chen J Z Y 2010 *Phys. Rev. E* **81** 011904
[36] Chen J Z Y and Mkrtchyan S 2010 *Phys. Rev. E* **81** 041906
[37] Chen J Z Y 2010 *Phys. Rev. E* **82** 060801
[38] Su Y C and Chen J Z Y 2013 *Soft Matter* **9** 570
[39] Deserno M, Müller M M and Guven J 2007 *Phys. Rev. E* **76** 011605
[40] Rodriguez-Garcia L R Arriaga, Mell M, Moleiro L H, Lopez-Monteroand Monroy F 2009 *Phys. Rev. Lett.* **102** 128101